HAL
open science

Synthesis, texture, and photoluminescence of lanthanide-containing chitosan-silica hybrids

Fengyi Liu, Luis D. Carlos, Rute A. Sa Ferreira, João Rocha, Marta C. Ferro, Audrey Tourrette, Françoise Quignard, Mike Robitzer

To cite this version:

Fengyi Liu, Luis D. Carlos, Rute A. Sa Ferreira, João Rocha, Marta C. Ferro, et al.. Synthesis, texture, and photoluminescence of lanthanide-containing chitosan-silica hybrids. Journal of Physical Chemistry B, 2010, 114 (1), pp.77-83. 10.1021/jp908563d . hal-00451362

HAL Id: hal-00451362

https://hal.science/hal-00451362v1

Submitted on 10 Dec 2021

HAL is a multi-disciplinary open access archive for the deposit and dissemination of scientific research documents, whether they are published or not. The documents may come from teaching and research institutions in France or abroad, or from public or private research centers.

L'archive ouverte pluridisciplinaire **HAL**, est destinée au dépôt et à la diffusion de documents scientifiques de niveau recherche, publiés ou non, émanant des établissements d'enseignement et de recherche français ou étrangers, des laboratoires publics ou privés.

Open Archive TOULOUSE Archive Ouverte (OATAO)
OATAO is an open access repository that collects the work of Toulouse researchers and makes it freely available over the web where possible.

This is an author-deposited version published in : http://oatao.univ-toulouse.fr/
Eprints ID : 4641

To link to this article : DOI:10.1021/jp908563d
URL : http://dx.doi.org/10.1021/jp908563d

To cite this version : Liu, F. and Carlos, L.D. and Ferreira, R.A. and Rocha, J. and Ferro, M.C. and Tourrette, A. and Quignard, F. and Robitzer, M. (2010) *Synthesis, texture, and photoluminescence of lanthanide-containing chitosan-silica hybrids*. The Journal of Physical Chemistry B, vol. 114 (n° 1). pp. 77-83. ISSN 1089-5647

Any correspondance concerning this service should be sent to the repository administrator: staff-oatao@inp-toulouse.fr.

Synthesis, Texture, and Photoluminescence of Lanthanide-Containing Chitosan−Silica Hybrids

Fengyi Liu,[†,‡] Luis D. Carlos,*[,†] Rute A. S. Ferreira,[†] João Rocha,[§] Marta C. Ferro,[||] Audrey Tourrette,[‡] Françoise Quignard,[‡] and Mike Robitzer*[,‡]

Department of Physics, CICECO, University of Aveiro, Portugal, Institut Charles Gerhardt-Montpellier, Matériaux Avancés pour la Catalyse et la Santé, UMR5253 CNRS-ENSCM-UM2-UM1, 8 rue de l'Ecole Normale, 34296 Montpellier, France, Departament of Chemistry, CICECO, University of Aveiro, Portugal, and Departament of Ceramics and Glass Engineering, CICECO, University of Aveiro, Portugal

Three different types of photoluminescent hybrid materials containing trivalent lanthanide (Ln^{3+} = Eu^{3+}, Tb^{3+}) ions, chitosan, and silica have been prepared with different structural features. The different silica sources lead to diverse microstructures of hybrid materials, with silica being homogeneously dispersed in the chitosan materials (**LnChS−H**), or forming a core−shell morphology. Postsynthesis treatment is necessary for embedding the luminescent probe. The Ln^{3+}-based materials have been investigated by photoluminescence spectroscopy (12−300 K). The chitosan−Eu^{3+}-related local environment is maintained in the **EuChS−H** hybrid material. The emission features of the core−shell materials are characterized by the presence of two Eu^{3+} distinct local environments, one associated with the chitosan core and the other with the silica shell.

I. Introduction

In the past decade, organic−(bio)−inorganic hybrid materials have gained much attention because these systems exhibit unique properties in many fields of applications, as they combine the respective characteristics of organic−(bio)−inorganic parts at the nanoscale.[1–3] In the field of optics, lanthanide-doped (essentially trivalent ions, Ln^{3+}) hybrids will play a key role in the development of advanced functional nanomaterials for a wide variety of potential applications, such as high efficiency and stable solid-state lasers, fluorescent labels, NIR-emitting probes, magnetic resonance imaging (MRI) contrast agents, optical fiber amplifiers, and devices with upconversion.[4–8] Their interest relies on the possibility of joint properties of sol−gel host materials (shaping, tunable refractive index and mechanical properties, corrosion protection, specific adhesion, etc.) and the well-known luminescence of Ln^{3+} ions (e.g., sharp 4f transitions, long lifetimes, and high-emission quantum yields). However, environmental requirements, such as recyclability and safety, must be taken into account in the future applications of these functional materials. Hence, the use of abundant, low cost, and environmentally friendly biopolymers, such as polysaccharides, to synthesize hybrid materials is gaining much attention.[9,10]

Chitosan is a biodegradable and biocompatible polysaccharide derived from chitin, a linear chain of acetylglucosamine groups, generally extracted from crab shell or squid pen (Scheme 1). Chitosan is obtained by removing most of the acetyl groups from chitin. This process gives rise to amine groups which can be used for further functionalization. Chitosan has many interesting features, including high affinities for dyes and metal ions,[11] and excellent process ability,[12] which makes it an ideal candidate for the preparation of functional hybrid materials.[13–17]

SCHEME 1: Molecular Structure of Chitin and Chitosan, Characterized by the Acetylation Degree AD = (*n*/(*m* + *n*))

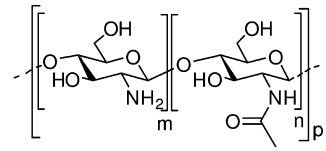

Chitin A.D. > 0.4; Chitosan A.D. < 0.4

In this paper, we wish to report the synthesis, texture, and photoluminescence of Ln^{3+}-containing chitosan−silica hybrids. Only a few papers report on the optical properties of Ln^{3+}-doped chitosan polymers, e.g., for waveguiding,[18] biological applications,[19] and cancer therapy.[20] However, to the best of our knowledge, no studies are available on the photoluminescence properties of Ln^{3+} chitosan−silica hybrids. In order to combine texture and photoluminescence properties, characterization measurements were done on the aerogel formulation[21] as the CO_2 supercritical drying stabilizing the polysaccharide gel porous network. Therefore, the synergy between the properties of chitosan, silica, and Ln^{3+} ions may pave the way to interesting multifunctional hybrid materials, especially for *in vivo* biological applications, combining the Ln^{3+} diagnostic local sensing features with the drug-delivery control of the chitosan−silica nanocomposites.

II. Experimental Section

Materials and Methods. The three types of hybrid materials studied are designated as **LnCh**, **LnChS−H**, **LnChS−CS** (**Ln**, lanthanide; **Ch**, chitosan; **S**, silica; **H** or **CS**, two different silica sources; **H**, TEOS (tetraethoxysilane) gives **H**omogenous structure; **CS**, Ludox colloidal silica (12 nm) gives **C**ore−**S**hell structure). The average diameter of the beads was 2.2 ± 0.1 mm.

* Corresponding authors. Fax: +351 234378197 (L.D.C); +33 467163470 (M.R.). Phone: +351 234370 946 (L.D.C); +33 467163494 (M.R.). E-mail: lcarlos@ua.pt (L.D.C); mike.robitzer@enscm.fr (M.R.).

[†] Department of Physics, University of Aveiro.

[‡] Institut Charles Gerhardt-Montpellier.

[§] Departament of Chemistry, University of Aveiro.

[||] Departament of Ceramics and Glass Engineering, University of Aveiro.

Preparation of chitosan gel beads (Ch). Chitosan solution was prepared by dissolving 1 g of chitosan (Aldrich from crab shell, degree of acetylation 10% as measured by IR spectroscopy,[22] M_w 700 000 Da) in 100 mL of a 0.055 M acetic acid solution. Total dissolution was obtained by stirring overnight at room temperature. Chitosan beads were obtained by dropping the chitosan solution into a 4 M NaOH solution through a 0.8 mm gauge syringe needle. The chitosan beads were left in the alkaline solution for 2 h, filtered, and washed with copious water. The hydrogel beads were successively immersed in a series of ethanol−water baths of increasing alcohol concentration (10, 30, 50, 70, 90, and 100%) for 30 min each to get the alcogel beads. The aerogel beads were obtained by drying under supercritical CO_2 conditions (slightly beyond 73.8 bar and 31.1 °C) in a Polaron 3100 apparatus.

***Preparation of* ChS−H.** These materials were prepared according to the published method.[23] A 2 g portion of chitosan alcogel beads (Ch) was introduced into a 25 mL Wheaton flask. A sol was formed after adding water (17 mL), TEOS (0.0566 mmol), and NaF (50 mg) to the flask. Mixing was ensured by rotation of the flask around its horizontal axis on a Heidolph Reacx2 stirrer for 12 h. The hybrid beads were then washed with water and exchanged with ethanol before supercritical CO_2 drying (slightly beyond 73.8 bar and 31.1 °C) in a Polaron 3100 apparatus.

Preparation of ChS−CS. A 10 mL portion of Ludox colloidal silica was added to a 25 mL Wheaton flask, and the pH was adjusted to 7.4. Then, 2 g of chitosan alcogel beads were introduced into the flask. Mixing was ensured by rotation of the flask around its horizontal axis on a Heidolph Reacx2. The thickness of the silica shell was controlled by the reaction time. The chitosan−silica composites with silica shells of ca. 200 and 550 μm have been prepared after 2 and 5.5 h reaction times, respectively. The hybrid beads were then washed with water. The alcogel beads were prepared after dehydration in a series of successive ethanol−water baths of increasing alcohol concentration (10, 30, 50, 70, 90, and 100%) for 30 min each. This system is denoted ChS−CS. Accordingly, the samples are named ChS−CS1 (Ch, chitosan; S, silica; CS, core−shell; 1, shell thickness 200 μm) and ChS−CS2 (2, shell thickness 550 μm).

***Preparation of* LnCh.** A 2 g portion of chitosan alcogel was added to a $LnCl_3$ solution (0.5 mmol of $LnCl_3$ in 15 mL of ethanol), kept for 1 day, and then washed with ethanol three times before drying with supercritical CO_2.

***Preparation of* LnChS−H.** A 2 g portion of chitosan−silica composite **ChS−H** alcogel was added to the solution of $LnCl_3$ (0.15 mmol of $LnCl_3$ in 15 mL of ethanol), washed with ethanol three times after 1 day, and then dried by supercritical CO_2.

Preparation of LnChS−CS. A 2 g portion of alcogel of chitosan core−shell materials (with different shell thicknesses) was added to the solution of $LnCl_3$/ethanol (0.15 mmol in 15 mL of ethanol) and kept for 1 day. Then, the beads were washed with copious ethanol. The alcogel beads were then dried under supercritical CO_2 conditions. The final samples were designated LnChS−CS1 (silica shell thickness of 200 μm) and LnChS−CS2 (silica shell thickness of 550 μm), respectively.

Characterization of Materials. ***Scanning electron micrographs*** of the aerogel microspheres were obtained using a Hitachi S-4500 apparatus after platinum metallization. Chemical composition (elemental maps) was measured on a Bruker AXS Quantax 400 energy dispersive X-ray spectrometry system (EDS) connected to a Hitachi SU-70 FEG-SEM apparatus. The samples for the analytical studies were coated with gold.

Nitrogen adsorption/desorption isotherms were recorded using a Micromeritics ASAP 2010 apparatus at 77 K after outgassing the sample at 323 K under a vacuum until a stable 3×10^{-3} Torr pressure was obtained without pumping. Surface areas were evaluated by the BET method assuming that a monolayer of N_2 molecules covers 0.162 nm^2/molecule.

Thermogravimetric analysis was performed with a Netzsch TG 209 C apparatus under air (20 mL min^{-1}, 25−850 °C, 5 °C min^{-1}) on a 10 mg sample.

Photoluminescence Spectroscopy. The photoluminescence spectra were recorded at 12 K and room temperature with a modular double grating excitation spectrofluorimeter with a TRIAX 320 emission monochromator (Fluorolog-3, Jobin Yvon-Spex) with a reciprocal linear dispersion density of 2.64 $nm \cdot mm^{-1}$ coupled with a R928 Hamamatsu photomultiplier, using the front face acquisition mode. The emission slits were fixed at 0.3 mm, enabling a resolution of 0.7 nm in the emission spectra. The excitation source was a 450 W Xe arc lamp. The emission spectra were corrected for detection and optical spectral response of the spectrofluorimeter, and the excitation spectra were corrected for the spectral distribution of the lamp intensity using a photodiode reference detector. The lifetime measurements were performed at 12 K and room temperature with the setup described for the luminescence spectra using a pulsed Xe−Hg lamp (6 μs pulse at half width and 20−30 μs tail). The absolute emission quantum yields were measured at room temperature using a quantum yield measurement system C9920-02 from Hamamatsu (experimental error 10%) with a 150 W xenon lamp coupled to a monochromator for wavelength discrimination, an integrating sphere as a sample chamber, and a multichannel analyzer for signal detection. Three measurements were made, and the average value is reported.

III. Results and Discussion

The preparation of the aerogel hybrid materials is a multistep process starting from chitosan alcogel spheres. In order to keep the porous texture of the hybrid materials, the supercritical drying technique was used which leads to an aerogel material. CO_2 is chosen because of its low critical point (31.1 °C at 73.8 bar). This technique is commonly used with inorganic solids to achieve very high specific surface area[24] and was successfully applied to polysaccharide gel.[21]

Dropping an acetic acid chitosan solution into the NaOH coagulation bath forms mechanically stable hydrogel spheres, which may be separated out of the synthesis bath. Chitosan alcogel spheres are, thus, obtained after exchange of water by ethanol through successive immersions in a series of ethanol−water baths of increasing ethanol concentration.

Two procedures of silica incorporation were used. The chitosan gel presents a very open macroporous texture with a void fraction as high as 99%. In the sol−gel procedure, this open texture allows an easy penetration of partially hydrolyzed ethoxysilane species into the core of the gel beads.[23] This leads to condensation of silica throughout the bead and formation of a homogeneous composite (**ChS−H**). In the second procedure, the composite (**ChS−CS**) is formed by aggregation of silica particles when the alcogel spheres of chitosan are reacted with Ludox colloidal silica. The resulting composites present a core−shell morphology. At this stage, the shell thickness may be tuned by changing the reaction time.

Different approaches may be used for the incorporation of Ln^{3+} ions within the porous network. The metal centers may be embedded either (i) before the silica incorporation, (ii) *in situ*, during the sol−gel processing, or (iii) by a postsynthesis

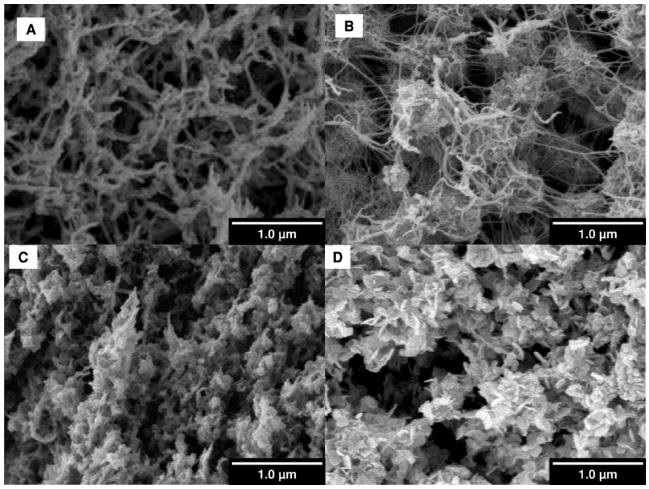

Figure 1. SEM pictures of the cross section of aerogels prepared using the procedure of Eu^{3+} incorporation: (A) chitosan; (B) Eu−Ch; (C) Eu−ChS−b−H; (D) Eu−ChS−"*in-situ*"−H.

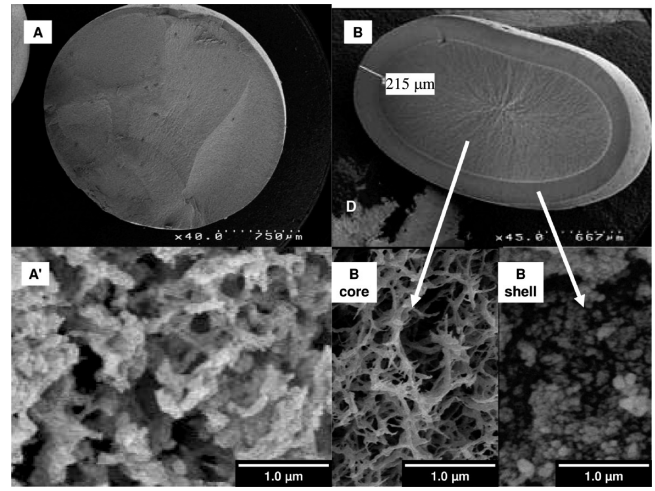

Figure 2. SEM of cross sections of EuChS−H (A, A′) and EuChS−CS (B, Bcore, Bshell).

treatment. In the first procedure, the Eu−chitosan alcogel hybrid (EuCh) is formed by impregnating the corresponding chitosan alcogel spheres with Ln^{3+} ethanol solution. This impregnation affects the structure of the chitosan network (Figure 1A and B). The diameters of chitosan fibrils are smaller, and the secondary structure adopts a "wind-into-a-ball" configuration. Then, the two previously described procedures for silica incorporation were carried out. Only the homogeneous route, with TEOS as the source of silica, afforded self-standing beads (**EuChS−b−H**). The morphology of the material was highly modified, as evidenced in the scanning electron microscopy (SEM) picture of the corresponding aerogels (Figure 1C), but the solid did not contain silica. In the *in situ* synthesis, the Ln^{3+} ions are introduced concomitantly with TEOS and NaF. Again, the spheres did not incorporate silica, and the SEM analysis of the aerogel revealed the presence of EuF_3 identified by EDS analysis (Figure 1D). As F^- is supposed to be the catalyst for silica condensation, the formation of EuF_3 prevents this catalytic reaction. The only way to obtain Ln^{3+}-doped chitosan−silica hybrid materials was by postsynthesis treatment of the previously synthesized hybrid materials.

Morphology and Textural Properties of the Eu^{3+}-Containing Chitosan−Silica Hybrid Aerogels. The two different morphologies of the Eu^{3+}-containing chitosan−silica hybrid materials are described in Figure 2. The homogeneous hybrid (Figure 2A) presents an open network of fibrils embedded with silica (Figure 2A′), as previously observed in absence of Eu^{3+}.[23] The core−shell hybrid presents the two different components (Figure 2B). The magnification reveals the presence of silica aggregates in the shell (Figure 2B shell) and the fibrillar structuring of chitosan in the core of the composite (Figure 2B core).

The localization of Eu^{3+} in the core−shell system was determined by X-ray mapping. Figure 3 depicts the mapping of the Si, Cl, and Eu elements, showing that the Si content is restricted to the shell. The Eu and Cl elements are essentially located within the core, Eu^{3+} ions being coordinated to the amine groups of chitosan. Europium and chloride are also present within the shell in a smaller amount. This behavior is independent of the thickness of the shell (**EuChS−CS1** and **EuChS−CS2** shell thickness of 220 and 550 μm, respectively), indicating that there is no diffusion limitation for $EuCl_3$ even in the silica shell.

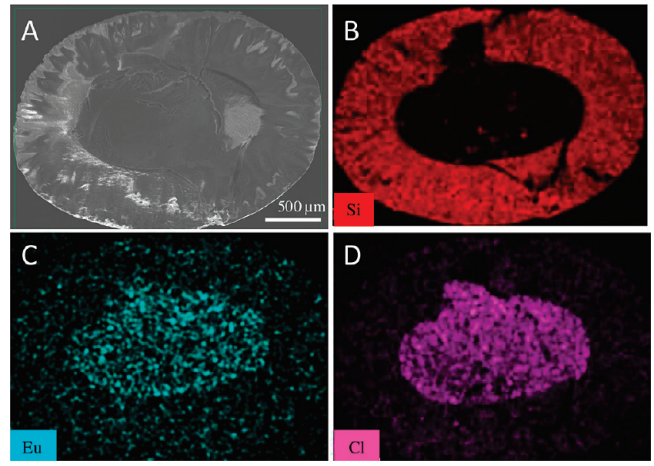

Figure 3. SEM of cross section micrographs of EuChS−CS2 (A). X-ray mapping of the relative Si, Eu, and Cl content in the shell and in the core (B, C, and D, respectively).

Nitrogen adsorption−desorption isotherms provided information on the textural properties of the aerogel core−shell hybrid materials dried by supercritical CO_2. Figure 4A compares the isotherms of chitosan aerogel with the two core−shell systems, **EuCh**, **EuChS−CS1**, and **EuChS−CS2**. All isotherms are essentially type II, corresponding to macroporous solids with high surface area. The BET surface area, 296 $m^2 \cdot g^{-1}$, of **EuCh** dropped to 209 $m^2 \cdot g^{-1}$ for **EuChS−CS1** and 227 $m^2 \cdot g^{-1}$ for **EuChS−CS2**, which shows that the porous texture of chitosan was kept intact during the silica incorporation procedure. It is noticeable that as the shell thickness increased the surface area of the aerogel hybrid materials increased slightly, which indicated that the porous structure is essentially derived from the chitosan core and that the shell is non-mesoporous. This is evidenced by the pore size distributions, very similar for all of the solids (Figure 4A). In contrast, in the sol−gel procedure, the porous texture of chitosan is lost and the **EuChS−H** isotherm is characteristic of a microporous material (Figure 4B).

Photoluminescence Spectroscopy. Figure 5A compares the excitation spectra of the Eu^{3+}-containing materials monitored within the $^5D_0 \rightarrow {}^7F_2$ transition in the range 12−300 K. At room temperature, the spectra are similar, showing a series of intra-$4f^6$ lines attributed to transitions between the $^7F_{0,1}$ levels and the $^5F_{1-5}$, $^5H_{3-7}$, $^5D_{4-1}$, $^5G_{2-5}$, and $^5L_6$ excited states superim-

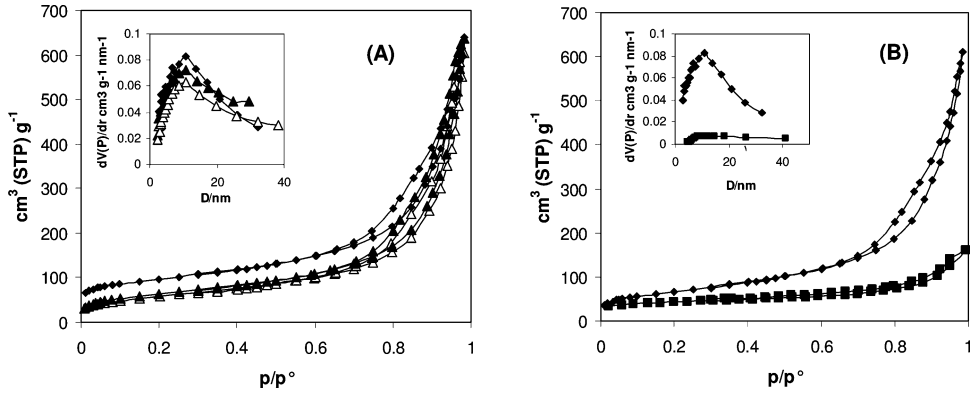

Figure 4. Nitrogen sorption isotherms of (A) EuCh (◆), EuChS−CS1 (△), and EuChS−CS2 (▲); (B) EuCh (◆), EuChS−H (■), and respective pore size distributions.

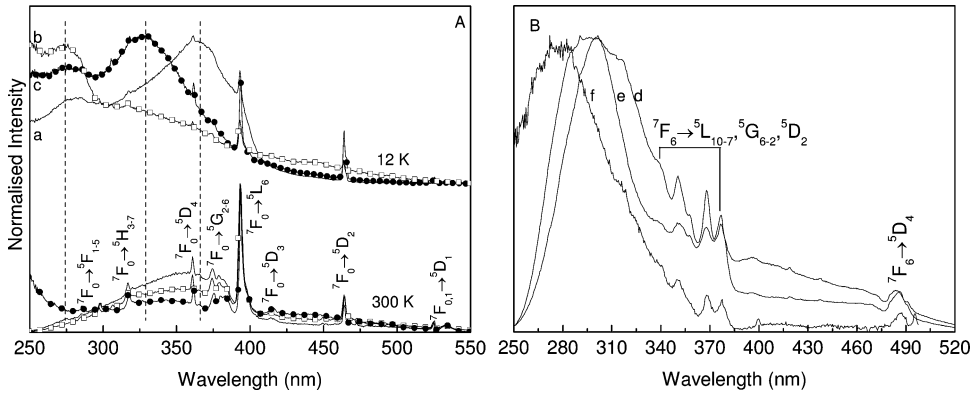

Figure 5. Excitation spectra acquired at 300 and 12 K for (A) (a) EuCh, (b) EuChS−H, and (c) EuChS−CS1 and (B) (d) TbCh, (e) TbChS−H, and (f) TbChS−CS monitored at 611 and 544 nm, respectively.

posed on a broad band at ca. 370 nm, characteristic of chitosan.[25] While the energy and full width at half-maximum (fwhm) of this band do not change for all of the materials, the relative intensity of the Eu^{3+} intra-$4f^6$ lines relative to that of the chitosan-related component depends on the composition of the material, being larger for the core−shell hybrids (**EuChS−CS1** and **EuChS−CS2**). This indicates that the Eu^{3+} sensitization *via* the chitosan-related states is less efficient compared to direct Eu^{3+} excitation. Decreasing the temperature to 12 K changes the Eu^{3+} excitation paths, increasing the relative intensity of the broad band and leading to the appearance of three components at 275, 330, and 370 nm, suggesting that such host-to-Eu^{3+}energy transfer mechanisms are thermally deactivated. Moreover, at 12 K, the relative intensities of the three components depend on the silica content. Whereas for the Eu^{3+}-doped chitosan (**EuCh**) the main excitation component is at ca. 370 nm, the silica inclusion in the EuChS−H material shifts the maximum excitation peak to the blue (275 nm). The **EuChS−CS1** core−shell hybrid displays a maximum excitation peak at 330 nm, as found at 300 K. The excitation spectra of the Tb^{3+}-doped samples were acquired at 300 K by monitoring within the $^5D_4 \rightarrow {}^7F_5$ transition. The spectra display a main large broad band superimposed on a series of Tb^{3+} intra-$4f^8$ lines ascribed to transitions between the $^7F_6$ level and the $^5L_{10-7}$, $^5G_{6-2}$, and $^5D_{4,2}$ excited states. In contrast with the Eu^{3+}-doped samples, the energy and fwhm of this broad band depend on the composition of the materials. For **TbCh** and **TbChS−H**, the band peaks at 300 nm and the fwhm is reduced ca. 30% in the excitation spectrum of the latter hybrid. For the **TbChS−CS** core−shell structure, the broad band is blue-shifted, peaking at ca. 277 nm. Such differences may be attributed to the contribution of the spin-forbidden (low-spin, LS, and high-spin, HS) interconfigurational fd transitions, discerned at ca. 240 and 280 nm, respectively.[26] It should also be noted that the sensitization process is more efficient for the **TbChS−CS**.

The overall emission features of the Eu^{3+}- and Tb^{3+}-containing materials strongly depend on the excitation wavelength and composition (Figure 6A and B, respectively). The emission consists of a strong broad band (380−680 nm) superimposed on a series of lines ascribed to the $^5D_0 \rightarrow {}^7F_{0-4}$ (Eu^{3+}) and $^5D_4 \rightarrow {}^7F_{6-1}$ (Tb^{3+}) transitions. For excitation between 300 and 420 nm, the intra-4f lines dominate, whereas for higher excitation wavelengths the broad band emission displays higher relative intensity. For all materials, the energy of such broad band emission shifts toward the red as the excitation wavelength increases. While the energy and fwhm of the broad band emission are similar for **Eu(Tb)Ch** and **Eu(Tb)ChS−H**, a broadening and red shift are observed for **Eu(Tb)ChS−CS**. As observed in the excitation spectra (Figure 5A), the broad component detected for **Eu(Tb)Ch** and **Eu(Tb)ChS−H** is related to chitosan. Increasing the shell thickness from 200 μm (**EuChS−CS1**) to 550 μm (**EuChS−CS2**) increases by 10% the relative intensity of the chitosan intrinsic emission, relative to that of Eu^{3+} (not shown).

The steady-state photoluminescence spectra of nondoped chitosan beads and core−shell material (**ChS−CS2**) were recorded to explore the effective host-to-Ln^{3+} interactions and to rationalize the above-mentioned variations in the broad band emission (namely, the appearance of a new component convoluted with the chitosan one) (Figure 7A). The chitosan excitation spectrum displays two components at ca. 290 and 375 nm. The excitation spectrum of **ChS−CS2** also exhibits another more intense band at ca. 400 nm. The component at 400 nm is also observed in the room-temperature emission spectra (Figure 7A).

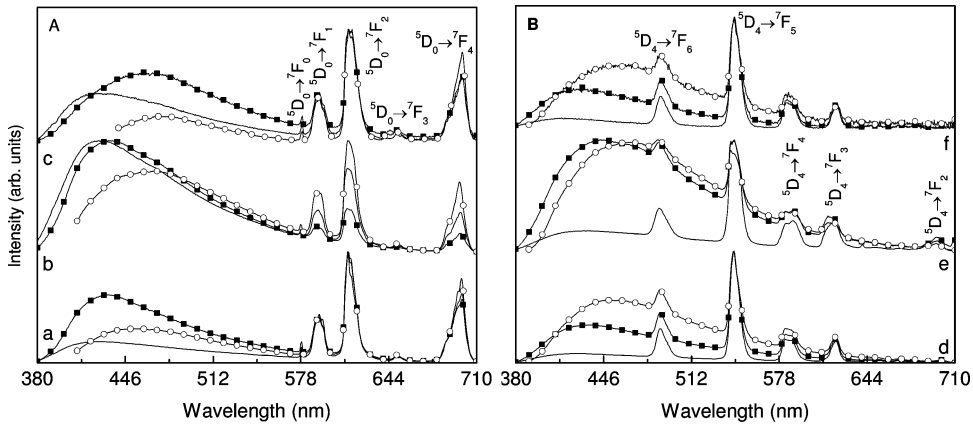

Figure 6. Room-temperature emission spectra of (A) (a) EuCh, (b) EuChS−H, and (c) EuChS−CS1 and of (B) (d) TbCh, (e) TbChS−H, and (f) TbChS−CS excited at (solid line) 317 nm, (open circles) 350 nm, and (solid squares) 393 nm.

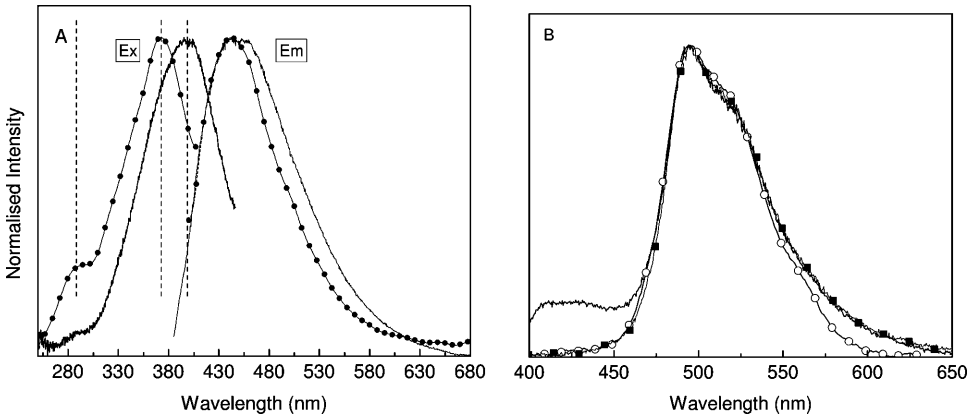

Figure 7. (A) Room-temperature excitation (Ex) and emission (Em) spectra of chitosan beads (solid line) and ChS−CS2 hybrid (solid line) monitored at 430 nm (chitosan beads) and 450 nm (ChS−CS2) and excited at 375 nm, respectively. (B) Time-resolved emission spectra (12 K) of ChS−CS2 excited at 380 nm acquired at distinct SD, (solid line) 0.05 ms, (squares) 5.00 ms, and (circles) 100.00 ms. The integration window was 20.00 ms.

In order to unambiguously establish the presence of these two distinct components in the core−shell hybrid materials, the emission spectra were acquired in time-resolved mode using different starting delays (SDs) (Figure 7B). The data were acquired at 12 K because at room temperature the time scale of the emission mechanisms is shorter than the detection limits of our equipment (10^{-5} s).

For SD values of 0.05 and 5.00 ms, the spectra consist, both, of a long-lived broad band with two components at ca. 495 and 520 nm and a high-energy band at ca. 425 nm. This latter component, not seen for higher SDs, resembles that observed in silicon-rich nanodomains in organic−inorganic hybrids.[27] The energy and time scale recombination mechanisms of the long-lived components are similar to those found for pure chitosan.[25] Clearly, the core−shell hybrids display emission contributions from both chitosan and amorphous silica.

Figure 8A shows the low-temperature high resolution emission spectra of Eu^{3+}-doped chitosan and hybrid materials. For the **EuCh** and **EuChS−H** samples, the Eu^{3+} intra-$4f^6$ emission lines display a broad profile well reproduced by a single Gaussian component for the nondegenerated $^5D_0 \rightarrow {}^7F_0$ transition and a maximum allowed splitting for the $^5D_0 \rightarrow {}^7F_{1,2}$ transitions, 3 and 5 components, respectively (Figure 8B−D). These observations and the higher relative intensity of the $^5D_0 \rightarrow {}^7F_2$ transition indicate that the Eu^{3+} local environment is characterized by a low symmetry group without an inversion center.

The emission spectra of **EuChS−CS1** and **EuChS−CS2** display two nondegenerated $^5D_0 \rightarrow {}^7F_0$ transitions (inset of

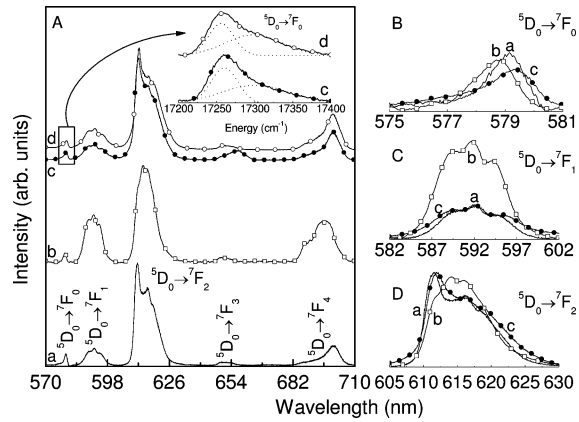

Figure 8. (A) Low-temperature (12 K) intra-$4f^6$ emission of the (a) EuCh, (b) EuChS−H, (c) EuChS−CS1, and (d) EuChS−CS2 materials excited at 280 nm. The inset shows in detail the $^5D_0 \rightarrow {}^7F_0$ line for the core−shell hybrids with the respective best fit using a sum of two Gaussian functions. (B, C, D) Detailed view of the $^5D_0 \rightarrow {}^7F_{0-2}$ transitions, respectively.

Figure 8). This is clear evidence for the presence of (at least) two Eu^{3+} local environments. In order to study in more detail the Eu^{3+} local environments, the energy and fwhm values (E_{00} and $fwhm_{00}$, respectively) of the nondegenerated $^5D_0 \rightarrow {}^7F_0$ transition were estimated.

The E_{00} and $fwhm_{00}$ values of EuCh (17268.9 ± 0.2 and 36.5 ± 0.7 cm^{-1}, respectively) and **EuChS−H** (17282.1 ± 0.3 and

TABLE 1: $^5D_0$ and $^5D_4$ Lifetime Values (τ, ms) for the Eu^{3+}- and Tb^{3+}-Containing Materials, Acquired at 300 and 12 K

	EuCh	EuChS−H	EuChS−CS1	EuChS−CS2	TbChS−CS1
300 K	0.169 ± 0.002	0.220 ± 0.004	0.157 ± 0.002	0.178 ± 0.002	0.839 ± 0.007
12 K			0.107 ± 0.007	0.152 ± 0.008	0.144 ± 0.007
	0.364 ± 0.002	0.278 ± 0.003	0.370 ± 0.006	0.360 ± 0.008	0.929 ± 0.011

42.2 ± 1.0 cm^{-1}) readily indicate different Eu^{3+}-coordinating shells that may involve a different type or number of Eu^{3+} first neighbors and/or changes in the average length of the Eu−ligand bonds. The relatively large $fwhm_{00}$ value of **EuChS−H** suggests a large distribution of closely similar Eu^{3+} local environments due to silica incorporation. The blue-shift in the E_{00} value of **EuChS−H** relative to the **EuCh** one (13.2 cm^{-1}) indicates an increase in the average covalency of the Eu^{3+}−ligand bonds.[28]

The E_{00} values of the low-energy $^5D_0 \rightarrow {}^7F_0$ lines of the core−shell hybrid materials (17260.3 ± 0.2 and 17258.0 ± 0.3 cm^{-1} for **EuChS−CS1** and **EuChS−CS2**, respectively, inset of Figure 8) are close to the **EuCh** value. Moreover, the similarity between the $fwhm_{00}$ values (33.5 ± 1.2 and 35.8 ± 0.9 cm^{-1}, respectively, for **EuChS−CS1** and **EuChS−CS2**) and the same relative intensity and energy of the $^7F_{1-4}$ Stark components suggest that the Eu^{3+} local environment with a low-energy $^5D_0 \rightarrow {}^7F_0$ line in the core−shell materials is similar to the one in **EuCh**. Further arguments supporting this suggestion will be raised when discussing the $^5D_0$ lifetimes (see below).

The Eu^{3+} local environment in **EuChS−CS1** and **EuChS−CS2** with higher E_{00} (17300.51 ± 1.4 and 17298.9 ± 1.0 cm^{-1}, respectively) and $fwhm_{00}$ (74.8 ± 3.6 and 90.4 ± 1.7, respectively) values is ascribed to the presence of Eu^{3+} in the shell. The integrated intensity of the high-energy $^5D_0 \rightarrow {}^7F_0$ line, relative to that of the low-energy one, increases ca. 10% in **EuChS−CS2**, compared with the value found for **EuChS−CS1** (inset in Figure 8A). This observation is related to the increase of the shell thickness (from 200 to 550 μm) and, consequently, to the increasing number of Eu^{3+}-related silica environments. At room temperature, the emission resembles that measured at 12 K, except for the core−shell hybrids where a single $^5D_0 \rightarrow {}^7F_0$ transition ascribed to the Eu^{3+} ions located in the core could be discerned. This result strongly suggests that the Eu^{3+} silica-related local environment is thermally quenched.

The emission decay curves of the $^5D_0$ (Eu^{3+}) and $^5D_4$ (Tb^{3+}) excited levels were measured at 612 and 544 nm, respectively, under direct intra-4f excitation ($^5L_6$, 395 nm, Eu^{3+} and $^7F_6$, 488 nm, Tb^{3+}) levels. For all of the materials, the decay curves were well fitted by a single exponential function, yielding the lifetime values gathered in Table 1. The similarity of the $^5D_0$ lifetime values (12 K) of **EuCh**, **EuChS−CS1**, and **EuChS−CS2** strengthens the above suggestion that one of the Eu^{3+} local environments in the core−shell hybrid structures is similar to that of chitosan, independently of the shell thickness. Comparing the $^5D_0$ lifetime temperature dependence between 12 and 300 K in **EuCh** and **EuChS−H**, a smaller decrease is observed for the hybrid (21 versus 46%). The smaller decrease of the nonradiative mechanisms in the hybrid is in agreement with the silica coating of the chitosan fibrils.[23] For the core−shell structure, the 12 K $^5D_0$ emission decay curves display a two-exponential behavior well modeled assuming that one of the lifetime values is coincident with that determined for **EuCh**. The Tb^{3+}-containing hybrid displays similar behavior, and the $^5D_4$ lifetime values are also listed in Table 1.

The quantum yield values of the Eu^{3+}- and Tb^{3+}-containing materials are below the detection limits of our equipment. To further interpret these poor quantum yield values, the $^5D_0$ radiative (k_r) and nonradiative (k_{nr}) transition probabilities and the quantum efficiency (η) [$\eta = k_r/(k_r + k_{nr})$] were estimated at room temperature, based on emission spectra and $^5D_0$ lifetime values (τ_{exp}).[5,29] The calculated values are gathered in Table 2. The k_{nr} value may be related to the number of water molecules and/or chitosan/silica hydroxyl groups (n_w) in the Eu^{3+} first coordination shell, through the empirical formula $n_w = 1.11 \times [\tau_{exp}^{-1} - k_r - 0.31]$[5,30] (Table 2). As expected, considering the large number of hydroxyl groups present on chitosan, silica, and water molecules, the q values are analogous and close to 4−6%. It is interesting to note that the higher q value found for **EuCHS−H**, relative to **EuCh**, is essentially due to the small nonradiative k_{nr} values, supporting the above suggestion of silica coating of the chitosan fibrils.[23]

TABLE 2: Radiative (k_r, ms^{-1}) and Nonradiative (k_{nr}, ms^{-1}) Transition Probabilities, Quantum Efficiency (η, %), and Number of Coordinated Water Molecules (and/or Chitosan/Silica Hydroxyl Groups) (n_w ± 0.1)

	k_r	k_{nr}	η	n_w
EuCh	0.287	5.630	4.8	5.9
EuCHS−H	0.264	4.282	5.8	4.4
EuChS−CS1	0.231	6.139	3.6	6.5
EuChS−CS2	0.254	5.240	4.6	5.5

IV. Conclusions

Three different types of photoluminescent bio−organic−inorganic hybrids containing Eu^{3+} or Tb^{3+} ions have been prepared. The microstructure of the hybrid materials may be tuned by silica incorporation, while the use of Eu^{3+} as a local probe has a strong influence on the hybrid synthesis. As a result, embedding the luminescent probe requires a post synthesis treatment. The Eu^{3+}- and Tb^{3+}-containing materials show the typical red and green emissions, respectively, overlapping with a broad emission ascribed to chitosan or chitosan and silica, for the hybrids. In the core−shell chitosan−silica hybrids, the Eu^{3+} probe resides in the chitosan core with a local coordination analogous to that found in the Eu^{3+}-doped chitosan. Relatively smaller amounts of Eu^{3+} ions are also present in the shell. A distinct emission, characteristic of a silica-related Eu^{3+} local coordination, is observed. The large number of coordinated hydroxyl groups in both environments results in similar $^5D_0$ quantum efficiency values (4−6%), independently of the structure of the materials. The local sensing features of these Ln^{3+}-containing chitosan−silica hybrids combined with their drug-delivery control may open innovative perspectives especially for *in vivo* biological applications in diagnostics and therapy.

Acknowledgment. We thank NoE "Functionalised Advanced Materials Engineering of Hybrids and Ceramics" (FAME), Fundação para a Ciência e Tecnologia, Portugal (BPD/26097/2005), FEDER, and PTDC for financial support.

References and Notes

(1) Sanchez, C.; Julian, B.; Belleville, P.; Popall, M. *J. Mater. Chem.* **2005**, *15*, 3559.

(2) Sanchez, C.; Lebeau, B.; Chaput, F.; Boilot, J.-P. *Adv. Mater.* **2003**, *15*, 1969.
(3) Sanchez, C.; Soller-Illia, G. J.; de, A. A.; Ribot, F.; Lalot, T.; Mayer, C. R.; Cabuil, V. *Chem. Mater.* **2001**, *13*, 3061.
(4) Escribano, P.; Lopez, B. J.; Arago, J. P.; Cordoncillo, E.; Viana, B.; Sanchez, C. *J. Mater. Chem.* **2008**, *18*, 23.
(5) Carlos, L. D.; Ferreira, R. A. S.; Bermudez, V. de Z.; Ribeiro, S. J. L. *Adv. Mater.* **2009**, *21*, 509.
(6) Comby, S.; Bünzli, J.-C. G. In *Handbook on the Physics and Chemistry of Rare Earths*; Gschneidner, K. A., Jr., Bünzli, J.-C. G., Pecharsky, V. K., Eds.; Elsevier: New York, 2007; pp 217−254.
(7) Le Quang, A. Q.; Zyss, J.; Ledoux, I.; Truong, V. G.; Jurdyc, A. M.; Jacquier, B.; Le, D. H.; Gibaud, A. *Chem. Phys.* **2005**, *318*, 33.
(8) Que, W. X.; Hu, X. *Appl. Phys. B* **2007**, *88*, 557.
(9) Coradin, T.; Allouche, J.; Boissiere, M.; Livage, J. *Curr. Nanosci.* **2006**, *2*, 219.
(10) Liu, F.; Carlos, L. D.; Ferreira, R. A. S.; Rocha, J.; Gaudino, M. C.; Robitzer, M.; Quignard, F. *Biomacromolecules* **2008**, *9*, 1945.
(11) Szyguła, A.; Guibal, E.; Ruiz, M.; Sastre, A. M. *Colloids Surf., A* **2008**, *330*, 219.
(12) Guibal, E. *Prog. Polym. Sci.* **2005**, *30*, 71.
(13) Peirano, F.; Vincent, T.; Quignard, F.; Robitzer, M.; Guibal, E. *J. Membr. Sci.* **2009**, *329*, 30.
(14) Nakamura, R.; Aoi, K.; Okada, M. *Macromol. Rapid Commun.* **2006**, *27*, 1725.
(15) Lu, X. B.; Wen, Z. H.; Li, J. H. *Biomaterials* **2006**, *27*, 5740.
(16) Darder, M.; Lopez-Blanco, M.; Aranda, P.; Aznar, A. J.; Bravo, J.; Ruiz-Hitzky, E. *Chem. Mater.* **2006**, *18*, 1602.
(17) Yamane, S.; Iwasaki, N.; Majima, T.; Funakoshi, T.; Masuko, T.; Harada, K.; Minami, A.; Monde, K.; Nishimura, S. *Biomaterials* **2005**, *26*, 611.
(18) Jiang, H.; Su, W.; Caracci, S.; Bunning, T. J.; Cooper, T.; Adams, W. W. *J. Appl. Polym. Sci.* **1996**, *61*, 1163.
(19) Wang, F.; Zhang, Y.; Fan, X.; Wang, M. *Nanotechnology* **2006**, *17*, 1527.
(20) Paeng, J. Y.; Kim, M. J.; Kang, J. H.; Shin, B. C.; Myoung, H. *Oral Oncol.* **2005**, *1*, 185.
(21) Quignard, F.; Valentin, R.; Di Renzo, F. *New. J. Chem.* **2008**, *32*, 1300.
(22) Hirai, A.; Odani, H.; Nakajima, A. *Polym. Bull.* **1991**, *26*, 17.
(23) Molvinger, K.; Quignard, F.; Brunel, D.; Boissiere, M.; Devoiselle, J. M. *Chem. Mater.* **2004**, *16*, 3367.
(24) Pierre, A. C.; Pajonk, G. M. *Chem. Rev.* **2002**, *102*, 4243.
(25) Silva, S. S.; Ferreira, R. A. S.; Fu, L.; Carlos, L. D.; Mano, J. F.; Reis, R. L.; Rocha, J. *J. Mater. Chem.* **2005**, *15*, 3952.
(26) (a) Laroche, M.; Doualan, J. L.; Girard, S.; Margerie, J.; Moncorgé, R. J. *J. Opt. Soc. Am. B* **2000**, *17*, 1291. (b) van Pierterson, L.; Reid, M. F.; Burdick, G. W.; Meijerink, A. *Phys. Rev. B* **2002**, *65*, 045114/1.
(27) Carlos, L. D.; Ferreira, R. A. S.; Bermudez, V. de Z.; Ribeiro, S. J. L. *Adv. Funct. Mater.* **2001**, *2*, 111.
(28) (a) Carlos, L. D.; Malta, O. L.; Albuquerque, R. Q. *Chem. Phys. Lett.* **2005**, *415*, 238. (b) Malta, O. L.; Batista, H. J.; Carlos, L. D. *Chem. Phys.* **2002**, *282*, 21.
(29) (a) Carlos, L. D.; Messaddeq, Y.; Brito, H. F.; Ferreira, R. A. S.; Bermudez, V. D.; Ribeiro, S. J. L. *Adv. Mater.* **2000**, *12*, 594. (b) Carlos, L. D.; Messaddeq, R. A. S.; Bermudez, V. D.; Ribeiro, S. J. L. *Adv. Mater.* **2009**, *21*, 509.
(30) Supkowski, R. M.; Horrocks, W. D. W., Jr. *Inorg. Chim. Acta* **2002**, *340*, 44.